Inorg. Chem. **2004**, *43*, 8049–8060

Structure and Bonding of the Vanadium(III) Hexa-Aqua Cation. 1. Experimental Characterization and Ligand-Field Analysis

Philip L. W. Tregenna-Piggott,* David Spichiger, Graham Carver, and Beatrice Frey

Department of Chemistry and Biochemistry, University of Bern, Freiestrasse 3, CH-3000, Bern 9 Switzerland

Roland Meier

Lehrstuhl für Anorganische und Analytische Chemie, Egerlandstrasse 1, 91058 Erlangen, Germany

Høgni Weihe

Institute of Chemistry, Universitetsparken 5, DK-2100 Copenhagen, Denmark

John A. Cowan and Garry J. McIntyre

Institut Laue-Langevin, BP156, 38042 Grenoble, Cedex 9, France

Gernot Zahn

Institut für Kristallographie und Festkörperphysik, Technische Universität Dresden, D-01062 Dresden, Germany

Anne-Laure Barra

Grenoble High Magnetic Field Laboratory, BP 166, 38042 Grenoble, Cedex 9, France

Received May 31, 2004

Spectroscopic and crystallographic data are presented for salts containing the $[V(OH_2)_6]^{3+}$ cation, providing a rigorous test of the ability of the angular overlap model (AOM) to inter-relate the electronic and molecular structure of integer-spin complexes. High-field multifrequency EPR provides a very precise definition of the ground-state spin-Hamiltonian parameters, while single-crystal absorption measurements enable the energies of excited ligand-field states to be identified. The EPR study of vanadium(III) as an impurity in guanidinium gallium sulfate is particularly instructive, with fine-structure observed attributable to crystallographically distinct $[V(OH_2)_6]^{3+}$ cations, hyperfine coupling, and ferroelectric domains. The electronic structure of the complex depends strongly on the mode of coordination of the water molecules to the vanadium(III) cation, as revealed by single-crystal neutron and X-ray diffraction measurements, and is also sensitive to the isotopic abundance. It is shown that the AOM gives a very good account of the change in the electronic structure, as a function of geometric coordinates of the $[V(OH_2)_6]^{3+}$ cation. However, the ligand-field analysis is inconsistent with the profiles of electronic transitions between ligand-field terms.

1. Introduction

Vanadium(III) complexes are the simplest systems in which to study the combined effects of a ligand field and interelectronic repulsion, and they continue to be the subject of intense theoretical study.[1−3] Advances in this area have, however, been hindered by the lack of experimental data to

* To whom correspondence should be addressed. E-mail: tregenna@iac.unibe.ch.

(1) Kallies, B.; Meier, R. *Inorg. Chem.* **2001**, *40*, 3101.
(2) Benmelouka, M.; Messaoudi, S.; Furet, E.; Gautier, R.; Le Fur, E.; Pivan, J.-Y. *J. Phys. Chem. A* **2003**, *107*, 4122−4129.

10.1021/ic049292l CCC: $27.50
Published on Web 11/03/2004

which theoretical models can be compared. This is largely because ions with integer-spins, such as vanadium(III), are often "silent" to conventional EPR spectroscopy, owing to the large zero-field-splitting of the ground state, inherent to non-Kramers ions. Recent years have seen a substantial effort to redress the dearth of experimental data. Electronic Raman[4,5] and luminescence[6,7] spectroscopies have been employed to yield the spinor-levels of the $^3T_{1g}$ (O_h) ground term, and single-crystal absorption spectroscopy applied to probe the levels of excited ligand field terms.[6,8−10] The determination of the ground-state spin-Hamiltonian parameters of integer-spin systems has traditionally been confined to the analysis of magnetic data.[11] Nowadays, the same information can be obtained more directly by the application of the inelastic neutron scattering[12] (INS) and high-field multifrequency EPR[13] (HF-EPR) techniques. In this work, EPR and electronic absorption spectroscopy are applied to study the $[V(OH_2)_6]^{3+}$ cation in a number of crystal structures. The spectroscopic data are complemented by crystallographic measurements, so setting a new standard for theoretical models that boast an ability to inter-relate the electronic and molecular structure of transition-metal complexes.

Data are presented for crystal structures of the general molecular formula $M^I[M^{III}(OX_2)_6](SO_4)_2$, where M^I is one of $[Cs(OX_2)_6]^+$, $[Rb(OX_2)_6]^+$, or $[C(NX_2)_3]^+$, X = H or D, and M^{III} is either vanadium(III), or a composite of vanadium(III) and a diamagnetic tervalent cation: aluminum(III), gallium(III), or indium(III). Throughout this work, a number of abbreviations are employed, representative examples of which are CsVSD, denoting $[Cs(OD_2)_6][V(OD_2)_6](SO_4)_2$, and Gu[Ga:V]SH, denoting vanadium(III) doped into $[C(NH_2)_3][Ga(OH_2)_6](SO_4)_2$, with Gu = guanidinium ion = $[C(NH_2)_3]^+$. These crystal systems were chosen as they are of high symmetry and are amenable to spectroscopic and crystallographic study. The X-ray structures of RbVSH,[14] CsVSH,[14,15] CsAlSH,[15] CsGaSH,[15] and CsInSH[15] have been reported previously. All have the β-alum structure in which the tervalent cation resides on sites of S_6 symmetry in a primitive cubic lattice. When the identity of the monovalent cation is changed from an alkali metal to the guanidinium cation, $[C(NH_2)_3]^+$, the space group changes from cubic ($Pa\bar{3}$) to trigonal ($P31m$), as revealed by X-ray diffractions studies of GuGaSH,[16] GuCrSH,[17] and GuAlSH.[17] In these ferroelectric guanidinium salts, there are two crystallographically distinct sites for the aqua ion to occupy, one of C_{3v} symmetry, the other C_3, present in the ratio 1:2. EPR studies of Cs[Al:V]SH,[18] GuVSH,[19−21] Gu[Al:V]SH[20,22] and Gu[Ga:V]SH[22] have been reported previously, though not using the range of fields and frequencies employed in the present study. The EPR spectra of Gu[Al:V]SH and Gu[Ga:V]SH have been discussed particularly extensively, owing to the peculiar fine structure, which has led one set of authors to suggest that the electron spin cannot be quantized along the symmetry axis,[22] an inference not supported by the data presented herein. It is shown that the single-crystal EPR data of Gu[Ga:V]SH are extremely instructive, with the extensive fine structure attributable to crystallographically distinct $[V(OH_2)_6]^{3+}$ cations, hyperfine coupling, and ferroelectric domains.

The AOM was developed to inter-relate the electronic and molecular structure of weakly covalent transition metal complexes, such as aqua ions. The data presented for the vanadium(III) hexa-aqua ion arguably provide the most rigorous test yet of the ability of the model to predict the electronic structure of a given complex knowing just the molecular structure and the AOM bonding parameters. The spectroscopic quantities are shown to depend strongly on the disposition of the hydrogen atoms, which define the stereochemistry of the $[V(OH_2)_6]^{3+}$ cation. The changes in the ground-state electronic structure brought about by substitution of $[Cs(OH_2)_6]^+$ for $[C(NH_2)_3]^+$ are indeed well accounted for by the AOM. However, the calculated energies of the components of excited ligand-field terms do not render an adequate explanation of the electronic Raman and electronic absorption band profiles.

2. Experimental Section

2.1. Synthesis. CsVSH,[15] RbVSH,[4] GuVSH,[5] CsAlSH,[15] CsGaSH,[15] CsInSH,[15] and GuGaSH[23] were prepared according to procedures previously described. Deuterated alums were prepared by repeated recrystallization (at least 3 times) from D_2SO_4 (1 M). Samples of Cs[Al:V]SX, Cs[Ga:V]SX, and Cs[In:V]SX, where X = H or D, were prepared by cocrystallization of the respective alums in solutions of X_2SO_4 (1 M) in which vanadium(III) constituted ca. 1% of the total tervalent-cation concentration.

2.2. Collection of Electronic Spectra. UV−vis−NIR spectra were recorded on a Cary 5e spectrometer at the Department of

(3) Anthon, C.; Bendix, J.; Schaffer, C. E.; *Inorg. Chem.* **2003**, *42*, 4088−4097.
(4) Tregenna-Piggott, P. L. W.; Best, S. P. *Inorg. Chem.* **1996**, *35*, 5730.
(5) Spichiger, D.; Carver, G.; Dobe, C.; Bendix, J.; Tregenna-Piggott, P. L. W.; Meier, R.; Zahn, G. *Chem. Phys. Lett.* **2001**, *337*, 391.
(6) Bussière, G.; Beaulac, R.; Cardinal-David, B.; Reber, C. *Coord. Chem. Rev.* **2001**, *219−221*, 509−543.
(7) Beaulac, R.; Tremblay, J. C.; Bussiere, G.; Reber, C. *Can. J. Anal. Sci. Spectrosc.* **2001**, *46* (5), 152−161.
(8) Tregenna-Piggott, P. L. W.; Best, S. P.; Güdel, H. U.; Weihe, H.; Wilson, C. C. *J. Solid State Chem.* **1999**, *145*, 460.
(9) Reber, C.; Beaulac, R. *Compr. Coord. Chem. II* **2004**, *2* 287−302.
(10) Landry-Hum, J.; Bussiere, G.; Daniel, C.; Reber, C. *Inorg. Chem.* **2001**, *40*, 2595−2601.
(11) Carlin, R. L. *Magnetochemistry*; Springer-Verlag: Berlin, 1986.
(12) Basler, R.; Tregenna-Piggott, P. L. W.; Andres, H.; Dobe, C.; Güdel, H.-U.; Janssen, S.; McIntyre, G. J. *J. Am. Chem. Soc.* **2001**, *123*, 3377. Carver, G.; Tregenna-Piggott, P. L. W.; Barra, A.-L.; Neels, A.; Stride, J. A.; *Inorg. Chem.* **2003**, *42*, 5771−5777.
(13) Smith, G. M.; Riedi, P. C. *Electron Paramagn. Reson.* **2000**, *17*, 164. Riedi, P. C.; Smith, G. M. *Electron Paramagn. Reson.* **2002**, *18*, 254.
(14) Beattie, J. K.; Best, S. P.; Del Favero, P.; Skelton, B. W.; Sobolev, A. N.; White, A. H. *J. Chem. Soc., Dalton Trans.* **1996**, 1481.
(15) Beattie, J. K.; Best, S. P.; Skelton, B. W.; White, A. H. *J. Chem. Soc., Dalton Trans.* **1981**, 2105.
(16) Geller, S.; Booth, D. P. *Z. Kristallogr.* **1959**, *111*, 117−128.
(17) Schein, B. J. B.; Lingafelter, E. C.; Stewart, J. M. *J. Chem. Phys.* **1967**, *47*, 2183.
(18) Clarke, J. G.; Mackinnon, J. A. *Can. J. Phys.* **1971**, *49*, 1539.
(19) McElearney, J. N.; Schwartz, R. W.; Merchant, S.; Carlin, R. L. *J. Chem. Phys.* **1971**, *55*, 466.
(20) Ashkin, J.; Vanderven, N. S. *Physica B* **1978**, *95*, 1−10.
(21) Diederix, K. M.; Groen, J. P.; Klaassen, T. O.; Poulis, N. J.; Carlin, R. L. *Physica* **1979**, *97B*, 113−125.
(22) Schwartz, R. W.; Carlin, R. L. *J. Am. Chem. Soc.* **1970**, *92*, 6763.
(23) Carver, G.; Bendix, J.; Tregenna-Piggott, P. L. W. *Chem. Phys.* **2002**, *282*, 245.

Table 1. Spin-Hamiltonian Parameters for the $[V(OH_2)_6]^{3+}$ Cation Doped into Various Diamagnetic Alums, Determined by EPR Spectroscopy

sample	D/cm^{-1}		$g_{\|\|}$	$g_\perp$	$A_{\|\|}$/cm^{-1}	$A_\perp$/cm^{-1}
Gu[Ga:V]SH	3.693(3) (C_{3v})	3.684(1) (C_3)	1.960(1)	1.895(1)	0.00991(2)	0.0110(5)
Cs[Ga:V]SH	4.8581(4)		1.9500(5)	1.8656(2)	0.0098(2)	0.0078(2)
Cs[Ga:V]SD	4.7735(2)		1.9549(1)	1.8690(2)	0.0099(1)	0.0078(2)
Cs[Al:V]SH	4.8713(1)		1.95188(3)	1.8662(4)	0.00988(4)	0.0080(6)
Cs[Al:V]SD	4.7813(2)		1.95308(5)	1.8700(2)	0.00985(7)	0.0081(3)
Cs[In:V]SH	4.8146(9)		1.9482(12)	1.8681(4)	0.0098(3)	0.0076(2)
Cs[In:V]SD	4.7348(5)		1.9490(8)	1.8714(6)	0.0098(2)	0.0077(3)

Chemistry, University of Bern. The polished crystals were sealed in a home-built copper cell and cooled to ca. 20 K using an Air Products closed-cycle refrigerator. For the cubic crystals of CsVSH, CsVSD, and RbVSH, unpolarized radiation was transmitted through faces of the type [111]. For the trigonal crystal of GuVSH, the electric vector of the polarized radiation was directed either parallel to (π-polarization) or perpendicular to (σ-polarization) the unique 3-fold axis of the crystal.

2.3. Collection of EPR Data. X-band spectra were recorded on a Bruker ELEXSYS spectrometer at the Department of Chemistry, University of Bern, in conjunction with an Oxford Instruments ESR 910 cryostat, automatic goniometer, and an ER 4116 DM dual-mode X-band resonator. Two small apertures were bored at the base at 60 mm from the base of the sample tube, to allow helium gas to pass over the sample. High-field, high-frequency EPR spectra were obtained at the Grenoble High Magnetic Field Laboratory. Excitation frequencies of ca. 95, 190, 285, 380, 115, 230, 345, and 460 GHz were employed in conjunction with a static field ranging from 0 to 12 T. Spectra were recorded between 5 and 20 K on single-crystal and powdered samples.

2.4. Collection of Crystallographic Data. Diffraction measurements were performed at the Institut Laue-Langevin (ILL), Grenoble, and at The Institute for Crystallography and Solid-State Physics, at the Technical University in Dresden, Germany.

2.4.1. Single-Crystal Neutron-Diffraction Data. Data for CsVSH and RbVSH were collected on the image-plate Laue diffractometer, LADI, at the ILL during a trial period on an unmonochromated thermal-neutron guide. Details of the instrument and the different steps in data analysis were described previously in the report on CsVSD.[32]

2.4.2. Single-Crystal X-ray Diffraction Data. Single-crystal X-ray diffraction measurements were carried out on a Rigaku AFC-7 three-circle/Mercury CCD diffraction system, equipped with a flat graphite-crystal monochromator, using Mo K radiation (0.71073 Å) at 292 K.

3.Results

3.1. EPR Spectra. Comprehensive data sets were obtained for the alkali metal vanadium alums, for the guanidinium vanadium alums, and for the corresponding diamagnetic alums containing vanadium(III) as an impurity. Data for RbVSH[8] and Cs[Ga:V]SX[24] have been communicated previously. All the EPR spectra were interpreted using the spin Hamiltonian for an axial (S, I) = (1, $^7/_2$) spin system

$$\hat{H}_s = g_{||}\beta B\cos\theta\hat{S}_z + g_\perp\beta B\sin\theta\hat{S}_x + A_{||}\hat{S}_z\hat{I}_z + A_\perp(\hat{S}_x\hat{I}_x + \hat{S}_y\hat{I}_y) + D\left\{\hat{S}_z^2 - \frac{1}{3}S(S+1)\right\} \quad (1)$$

which is valid for the ^3A_g (S_6) component of $^3T_{1g}$ (O_h) being much lower in energy compared to ^3E_g (S_6). The parameters $g_{||}$, $g_\perp$, $A_{||}$, $A_\perp$, and D were extracted from the spectra obtained for CsVSH, CsVSD, GuVSH, GuVSD, RbVSH, Cs[Ga:V]SH, Cs[Ga:V]SD, Cs[Al:V]SH, and Cs[Al:V]SD, by solving the spin-Hamiltonian (eq 1) numerically, utilizing the EPR simulation program SIM,[25] and minimizing the function

$$\chi^2 = \sum_{i=1}^{N}\left[\frac{B_{\mathrm{obs},i} - B_{\mathrm{calc},i}}{\sigma_i}\right]^2 \quad (2)$$

where N is the number of observations, $B_{\mathrm{obs},i}$ and $B_{\mathrm{calc},i}$ are the ith observed and calculated resonance magnetic fields, respectively, and σ_i is the measurement error associated with the ith resonance magnetic field. With the exception of RbVSH,[8] hyperfine structure could be resolved only for the doped crystal systems. The results are presented in Tables 1 and 2. The error bars are those from the least-squares refinement and pertain to the relative precision of the spin-Hamiltonian parameters and not the absolute accuracy. The parameters D, $g_{||}$, and $g_\perp$ can be determined with an accuracy no greater than the g value of DPPH ($g = 2.0036(1)$) against which the field was calibrated.

A total of nine and seven resonances were used to determine the spin-Hamiltonian parameters of CsVSH and CsVSD, respectively. There is no indication of any deviation from axial symmetry for either system, the resonances corresponding to the external magnetic field being either parallel or perpendicular to the S_6 axis of the vanadium(III) cation. An EPR study of GuVSH has been reported previously, at a frequency of 21 GHz, and the following spin-Hamiltonian parameters determined:[20] $D = 3.85(1)$ cm^{-1}, $g_{||} = 2.00(2)$, $g_\perp = 1.91(2)$. Our data are broadly consistent with these parameters. The band profiles of GuVSH and GuVSD were extremely complex, which may, in part, be due to the two crystallographically inequivalent complexes. Attempts to deconvolute the band profile into resonances that could be assigned to complexes on either the C_3 or C_{3v}

(24) Tregenna-Piggott, P. L. W.; Weihe, H.; Bendix, J.; Barra, A.-L.; Güdel, H.-U. *Inorg. Chem.* **1999**, *38*, 5928.
(25) Weihe, H. *SIM*; Department of Chemistry, University of Copenhagen: Copenhagen.
(26) Tregenna-Piggott, P. L. W.; Noble, C. J.; Pilbrow, J. R. *J. Chem. Phys.* **2000**, *113*, 3289−3301.
(27) Pilbrow, J. R. *Transition Ion Electron Paramagnetic Resonance*; Clarendon Press: Oxford, 1990; pp 287−289.
(28) Johnson, D. A.; Nelson, P. G. *Inorg. Chem.* **1999**, *38*, 4949.
(29) Walker, I. M.; Carlin, R. L. *J. Chem. Phys.* **1967**, *46*, 3931−3936.
(30) Matthewman, J. C.; Thompson, P.; Brown, P. J. *J. Appl. Crystallogr.* **1982**, *15*, 167.
(31) Becker, P.; Coppens, P. *Acta Crystallogr.* **1974**, *A30*, 129.
(32) Tregenna-Piggott, P. L. W.; Andres, H. P.; McIntyre, G. J.; Best, S. P.; Wilson, C. C.; Cowan, J. A. *Inorg. Chem.* **2003**, *42*, 1350.

Table 2. Spectroscopic Parameters for the Vanadium Alums

exptl technique	quantity determined	RbVSH	CsVSH	CsVSD	GuVSH	GuVSH	GuVSD
EPR	spin-Hamiltonian parameters of ^3A_g (S_6) ground term	$D = 4.906(4)$ cm^{-1} $g_\parallel = 1.944(1)$ $g_\perp = 1.863(2)$	$D = 4.87(1)$ cm^{-1} $g_\parallel = 1.947(7)$ $g_\perp = 1.868(4)$	$D = 4.79(2)$ cm^{-1} $g_\parallel = 1.95(2)$ $g_\perp = 1.869(6)$	$D = 3.73(5)$ cm^{-1} $g_\parallel = 1.94(2)$ $g_\perp = 1.91(2)$		$D = 3.73(9)$ cm^{-1} $g_\parallel = 1.95(3)$ $g_\perp = 1.90(2)$
electronic Raman spectroscopy	transition between trigonal components ($^3A_g \rightarrow {}^3E_g$) of $^3T_{1g}$ (O_h) ground term	1930(10) cm^{-1}	1940(10) cm^{-1}		C_{3v} 2650, 2719, ~2797 cm^{-1}	C_3 2667, 2737, ~2797 cm^{-1}	~2786, ~2860, ~2954 cm^{-1}[b]
	transition between ^3A_g and ^1E_g (S_6) ligand field terms	10204(2) cm^{-1}	10213(1) cm^{-1}	10227(1) cm^{-1}	10199(15)[c]		
electronic absorption and luminescence spectroscopy[a]	transition between $^3T_{1g}$(F) and $^3T_{2g}$ (O_h) ligand field terms	17600(400) cm^{-1} 19900(800) cm^{-1}	17700(400) cm^{-1} 20200(800) cm^{-1}	18000(1000) cm^{-1} 20000(1000) cm^{-1}	16700, 18900, 21000 cm^{-1} (σ) 19000, 22000 cm^{-1} (π)		
	transition between $^3T_{1g}$(F) and $^3T_{1g}$(P) (O_h) ligand field terms	25500(100) cm^{-1} 27800(400) cm^{-1}	25400(100) cm^{-1} 27800(400) cm^{-1}	25500(200) cm^{-1} 27400(700) cm^{-1}	27700, 29500 cm^{-1} (σ) 25600, 27000, 29000, 29800 (π)		

[a] The band positions for the alkali-metal alums were obtained by least-squares fitting of the band profiles to a superposition of Gaussian functions. The band positions listed for the guanidinium alum simply correspond to the energies of prominent features identified in the spectrum. [b] Unpublished data. [c] Taken from ref 7.

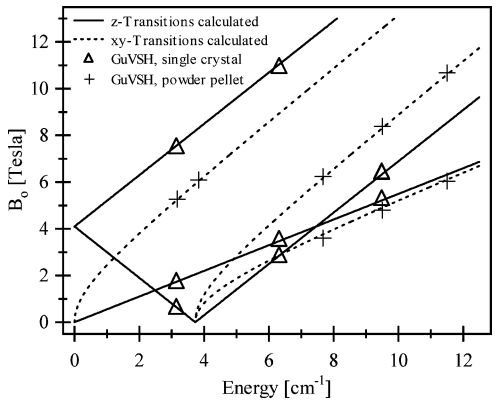

Figure 1. Experimental and calculated resonant-field positions of GuVSH.

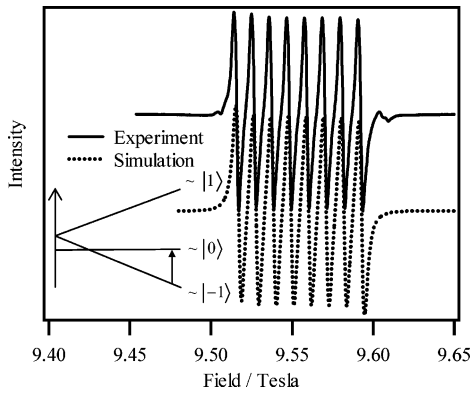

Figure 2. Representative single-crystal EPR spectrum of Cs[Al:V]SH recorded at 114.9994 GHz with the [111] direction of the crystal aligned along B_0 ($\theta = 0°$) at 6 K. The spectral simulation is shown as a broken line and was calculated using the spin-Hamiltonian parameters given in Table 1.

sites proved inconclusive. Hence, the mean of position of the profile was used as input to the least-squares refinement, which meant that the spin-Hamiltonian parameters were determined with a precision poorer than that of the alkali-metal vanadium alums. In Figure 1, the resonance positions of GuVSH are plotted against the microwave energy. Good agreement is obtained with the theoretical relation, calculated with the spin-Hamiltonian parameters given in Table 2.

A representative single-crystal EPR spectrum of Cs[Al:V]SH is shown in Figure 2 along with a simulation calculated with the corresponding spin-Hamiltonian parameters given in Table 1. The spectrum shows the characteristic eight-line spectrum arising from hyperfine coupling with the $I = {}^7/_2$ ^{51}V nucleus and is assigned to the $M_s = -1 \rightarrow M_s = 0$ transition, as depicted in the inset. Agreement between the experimental and simulated spectrum is seen to be excellent. The data sets obtained for Cs[In:V]SH and Cs[In:V]SD were not as extensive, but the spin-Hamiltonian parameters were nevertheless determined precisely.

For all samples, the improvement in the agreement between experimental and simulated spectra upon including the rhombic term, $E\{\hat{S}_x^2 - \hat{S}_y^2\}$, and letting g_{xx} differ from g_{yy}, was not found to be significant. However, evidence for disorder was discerned in spectra of Cs[Al:V]SX and Cs[In:V]SX, where the mismatch between the ionic radii of the host- and dopant-tervalent cation is acute, but not in the spectra of Cs[Ga:V]SX, where the ionic radii of the host and dopant ions are very similar. Figure 3 displays the X-band spectrum of Cs[Al:V]SH with a [111] direction of the crystal aligned parallel to the external field, B_0, and the microwave field, B_1, also polarized parallel to B_0. In this configuration, the parallel-mode EPR spectrum of the $[V(OH_2)_6]^{3+}$ cation, for which $\theta = 0°$, is a very sensitive measure of low-symmetry distortions. With $h\nu \gg E$, and ignoring the hyperfine term in the Hamiltonian (eq 1), the following expressions can be derived using standard methods of perturbation theory, for the resonant-field position, B(res), and transition probability in parallel mode, W_{23}, between the two levels, which in zero-field lie at an energy, $\sim D$, above the ground state

$$B_{\theta = 0°}(\text{res}) \approx \frac{h\nu}{2g_\parallel\beta} - \frac{E^2}{g_\parallel\beta h\nu} \quad (3)$$

$$W_{23} \approx \left(\frac{E}{\beta B(\text{res})}\right)^2 \quad (4)$$

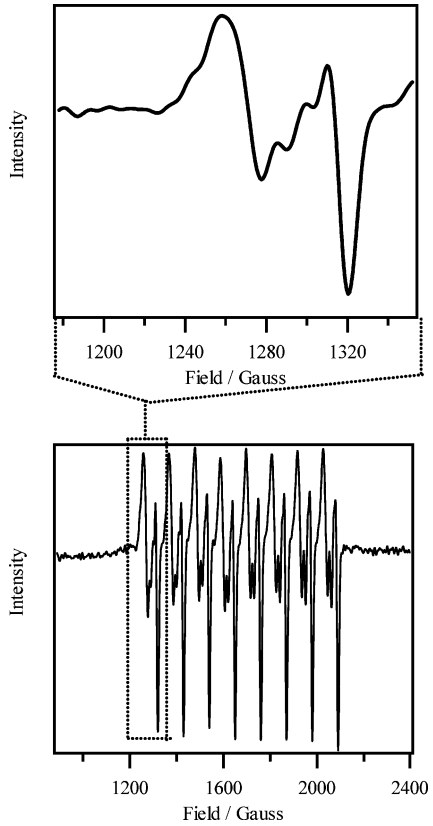

Figure 3. X-band, 9.312117 GHz EPR spectrum of Cs[Al:V]SH with $\theta = 0°$, and B_1 parallel to B_0.

Due to deviations from axial symmetry, the resonance positions are found at lower field values with ever greater transition probability, these modifications being quadratic in the rhombic spin-Hamiltonian parameter, E. The parallel-mode spectrum, presented in Figure 3, is indicative of the coexistence of a number of $[V(OH_2)_6]^{3+}$ species in the Cs[Al:V]SH crystal, which may be distinguished by the differing values of the parameter, E. Recently, we reported a detailed study of the EPR spectrum of Cs[Al:Ti]SH.[26] Although the physics of the system is completely different, there too, with [111] aligned parallel to B_0, low-symmetry distortions give rise to a shift of the EPR spectrum to lower field, and an increase in the transition probability. The EPR spectrum in the insert of Figure 3 is remarkably similar to that of Cs[Al:Ti]SH, suggesting that the spectrum is indicative of the statistical possibilities of accommodating a tervalent cation whose ionic radius is much larger than that of aluminum(III) and is not governed strongly by the detailed electronic structure of the dopant ion.

Of all the EPR spectra collected, those of Gu[Ga:V]SH were the most aesthetically pleasing, and proved to constitute an extremely instructive study of the EPR spectra of hexacoordinate vanadium(III) complexes. We take the liberty, therefore, of describing the spectra in some detail. The spectra obtained using the HFEPR setup at the GHMFL were recorded on a single crystal with the 3-fold axis aligned as close as possible along the direction of the applied field. In Figure 4 is shown the EPR spectrum, collected at ~115 GHz. Extensive structure is observed, which can be deconvoluted into two overlapping sets, consisting of eight equidistantly

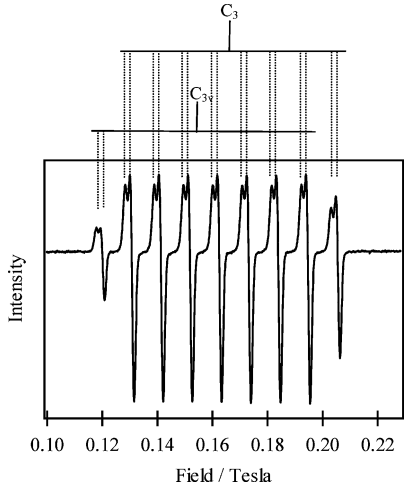

Figure 4. Single-crystal EPR spectrum of Gu[Ga:V]SH, recorded at 5 K, with an excitation frequency of 114.9784 GHz, and with the trigonal axis parallel to the external field.

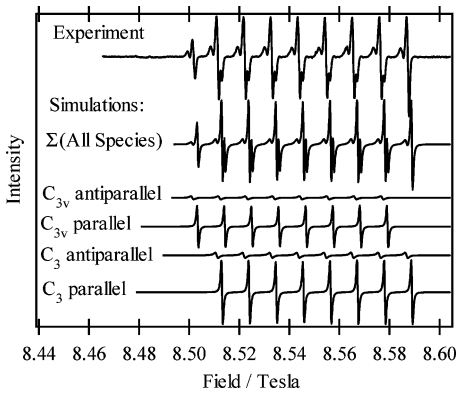

Figure 5. Single-crystal EPR spectrum of Gu[Ga:V]SH, recorded at 5 K, with an excitation frequency of 344.9352 GHz, and with the trigonal axis parallel to the external field. Also shown is a simulated spectrum, constructed as the sum of four spectra. Each calculated subspectrum corresponds to one of the two crystallographically inequivalent $[V(OH_2)_6]^{3+}$ species in different orientations of ferroelectric domains parallel and antiparallel to the *c*-axis of the trigonal unit cell. The spectra were scaled with the intensity ratios $C_{3v}(a)/C_{3v}(p)/C_3(a)/C_3(p) = 1:3:2:6$, and were calculated with $g_{||} = 1.960$ and values for the parameter D of $C_{3v}(a)$, 3.692 cm^{-1}; $C_{3v}(p)$, 3.695 cm^{-1}; $C_3(a)$, 3.683 cm^{-1}; $C_{3v}(p)$, 3.685 cm^{-1}. The bandwidth for the transitions designated "antiparallel" was set to a value three times larger than that for the transitions designated "parallel".

spaced resonances, with an intensity ratio of 2:1. Within the GuGaSH crystal, there are two sites of C_3 for every one of C_{3v} symmetry, which a tervalent cation can occupy. The spectra are consistent with a statistical distribution of $[V(OH_2)_6]^{3+}$ complexes in the Gu[Ga:V]SH crystal. The more intense eight-line spectrum is assigned to the $[V(OH_2)_6]^{3+}$ cations on sites of C_3 symmetry, and the less intense eight-line spectrum to the $[V(OH_2)_6]^{3+}$ cations on sites of C_{3v} symmetry. Each resonance is split further into a doublet, an observation which is not uncommon for EPR spectra of $S > {}^1/_2$ systems in a ferroelectric crystal.[27] The consequence of the ferroelectric phase is to modify the effective trigonal field at the vanadium(III) site. We attribute the additional structure to $[V(OH_2)_6]^{3+}$ species in different orientations of ferroelectric domains parallel or antiparallel to the *c*-axis of the trigonal unit cell, giving rise to two values of the parameter D for each of the crystallographically distinct $[V(OH_2)_6]^{3+}$ cations. In Figure 5 it is demonstrated how the EPR spectrum

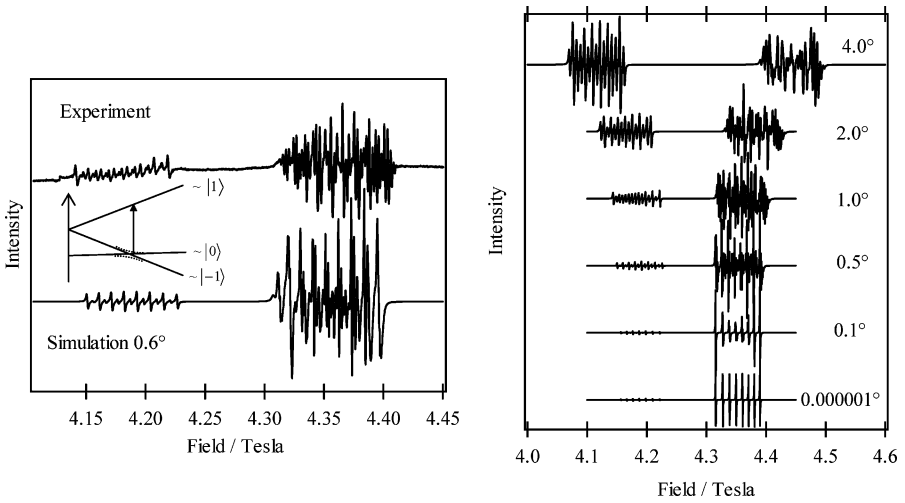

Figure 6. Experimental and calculated EPR spectra of Gu[Ga:V]SH, at 5 K and 229.9568 GHz. Spectra were calculated using the spin-Hamiltonian pertaining to the C_{3v} site, given in Table 1, as a function of the deviation of the quantization axis from the direction of the external field.

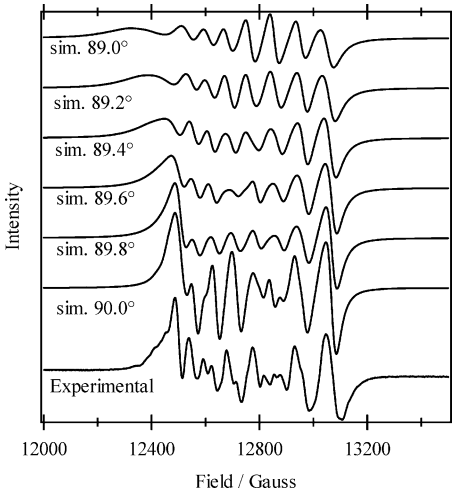

Figure 7. Experimental and simulated X-band EPR spectra of Gu[Ga:V]SH as a function of the deviation of the principal axis from B_0. The spectrum was recorded at 5 K and ca. 9.6 GHz, with the B_1 field polarized perpendicular to B_0. The simulations were calculated using the spin-Hamiltonian parameters given in Table 1.

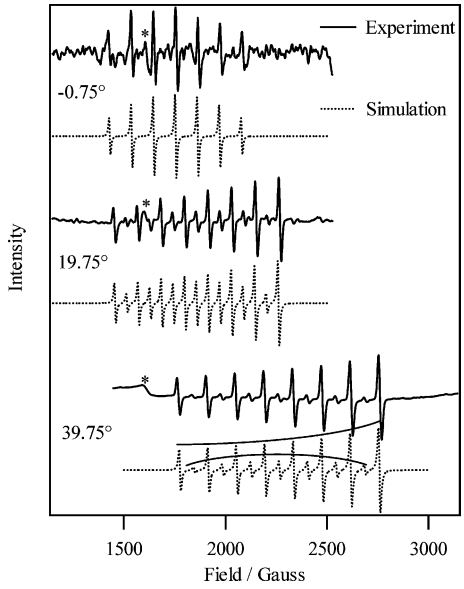

Figure 8. X-band EPR spectra of Gu[Ga:V]SH recorded at 5 K and ca. 9.6 GHz, with the B_1 field polarized perpendicular to B_0, as a function of θ. The simulations were calculated using the spin-Hamiltonian parameters pertaining to the C_3 complex given in Table 1. The feature marked with an asterisk is a resonance of the empty cavity. The two curves superimposed on the bottom spectrum illustrate how the intensities obtained from perturbation theory match the profiles of the two sets of peaks in the bottom spectrum, see eqs 8 and 9.

recorded at ~345 GHz can be constructed as the sum of four spectra calculated with different values of D. In this example, a ratio of "parallel" to "antiparallel" $[V(OH_2)_6]^{3+}$ species of 3:1 gave the best reproduction of the experimental data. The reproduction of spectra at other field positions required alternative values for this ratio.

The spectra recorded at ~230 GHz allowed the orientation of the principal axis with respect to the external field to be determined precisely. With $\theta = 0°$, there occurs a level crossing of the $|-1\rangle$ and $|0\rangle$ levels at ~4 T, as depicted in Figure 6. It was then fortunate that the energy difference to the higher lying $|1\rangle$ state is close to 230 GHz, one of the frequencies available from the Gunn diode. Mixing of the $|-1\rangle$ and $|0\rangle$ levels, through the external field, occurs when $\theta \neq 0°$, resulting in two sets of resonances whose field positions and relative intensities depend strongly on the value of θ, as shown in Figure 6. Comparison of experimental and calculated spectra resulted in a value for θ of 0.6(1)°.

In Figures 7 and 8 are shown single-crystal EPR spectra of Gu[Ga:V]SH, recorded at X-band with $B_1 \perp$ to B_0. The crystal was mounted on a quartz sample holder with the unique 3-fold axis and the direction of the external field defining a plane perpendicular to the axis of rotation. In Figure 7, an experimental spectrum is presented along with simulated spectra, calculated with one set of spin-Hamiltonian parameters, for values of θ close to 90°. From comparison between theory and experiment, we may infer that the alignment of the crystal is such that θ is within 0.2° of 90°. The resonance positions were best reproduced with $g_\perp$ set to 1.895(1) and $A_\perp$ set to 0.0110(5) cm^{-1}. In Figure 8 is shown the experimental spectrum with $\theta = -0.75(5)°$. In order to explain the spectra of Gu[Al:V]SH and Gu[Ga:V]SH with $\theta \sim 0°$, Schwartz and Carlin[22] had to invoke a model in which the Zeeman and hyperfine tensors were not collinear. However, the spectrum in Figure 9 of

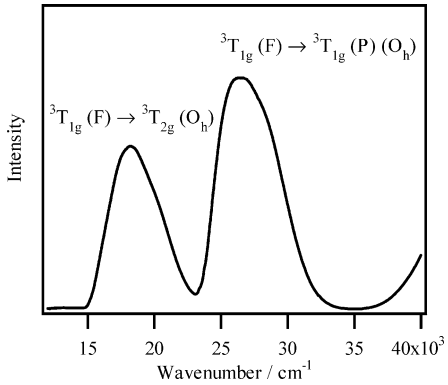

Figure 9. Single-crystal UV−vis spectrum of CsVSH between 12000 and 40000 cm^{-1}, collected at 16 K.

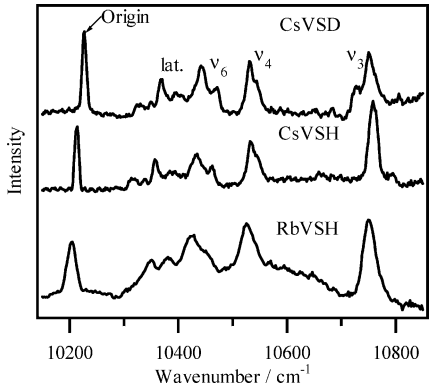

Figure 10. Single-crystal NIR spectra of CsVSD, CsVSH, and RbVSH, collected at ca. 16 K. The bandwidths of the zero-phonon lines (origin) are determined by the instrumental resolution.

their paper has a greater similitude with spectra we have collected for values of θ somewhat greater than 0°. The angular dependence of the EPR spectra of Gu[Ga:V]SH can be understood assuming that the zero-field-splitting, hyperfine, and Zeeman tensors are all collinear, using standard methods of perturbation theory.

The Hamiltonian (eq 1) may be rewritten as

$$\hat{H}_s = \hat{H}_0 + \hat{H}_1 + \hat{H}_2 \tag{5}$$

where

$$\hat{H}_0 = D\left\{\hat{S}_z^2 - \frac{1}{3}S(S+1)\right\} + g_{||}\beta B\cos\theta\hat{S}_z + A_{||}\hat{S}_z\hat{I}_z$$

$$\hat{H}_1 = g_\perp\beta B\sin\theta\hat{S}_x$$

$$\hat{H}_2 = A_\perp(\hat{S}_x\hat{I}_x + \hat{S}_y\hat{I}_y)$$

Under the conditions in which the X-band experiments were performed, $\hat{H}_0$ is the dominant term and is diagonal in the $|M_s, M_I\rangle$ basis. Treating $\hat{H}_1$ and $\hat{H}_2$ as simultaneous perturbations to $\hat{H}_0$ in the limit where θ is small, a spectrum consisting of 15 lines is predicted, the resonance fields for which are

$$\text{set of eight lines: } B(\text{res}) \approx \frac{h\nu - lA_{||}}{2g_{||}\beta\cos\theta} \quad l = 7{,}5{,}3...-7 \tag{6}$$

$$\text{set of seven lines: } B(\text{res}) \approx \frac{h\nu - mA_{||}}{2g_{||}\beta\cos\theta} \quad m = 6,\ 4,\ 2...-6 \tag{7}$$

The set of eight lines obtain intensity from the component of the magnetic field perpendicular to the principal axis:

$$W(\text{set of eight lines:}) \approx \frac{g_\perp{}^3\beta^2 B(\text{res})^2\sin^2\theta}{D^2} \tag{8}$$

The set of seven lines obtain intensity from the off-diagonal hyperfine interaction:

$$W(\text{set of seven lines}) \approx n\left(\frac{g_\perp A_\perp}{D}\right)^2, \text{ where } \begin{matrix} m & 6 & 4 & 2 & 0 & -2 & -4 & -6 \\ n & 7 & 12 & 15 & 16 & 15 & 12 & 7 \end{matrix} \tag{9}$$

More information on the energies and wave functions of the states is given in Supporting Information. The resonance positions and transition probabilities are in accordance with the theoretical spectra presented in Figure 8, which were calculated by full matrix diagonalization of the Hamiltonian (eq 1).

It is seen that the ground-state spin-Hamiltonian parameters of the $[V(OH_2)_6]^{3+}$ cation are very sensitive to the crystal environment. The zfs is significantly lower when guanidinium is the countercation; a small change in the value of D is also observed when cesium is replaced by rubidium. The change in the spin-Hamiltonian parameters upon deuteriation is seen to be quite significant, with a reduction in the parameter, D, of 0.08(2), 0.0900(2), 0.0846(4), and 0.0798(10) cm^{-1} for CsVSH, Cs[Al:V]SH, Cs[Ga:V]SH, and Cs[In:V]SH, respectively. The g values are also seen to be affected by deuteriation, the increase in $g_{||}$ for the Cs[Ga:V]SH system being particularly marked. The hyperfine coupling constants are found to be insensitive to isotopic substitution.

3.2. Electronic Spectra. The electronic spectrum of CsVSH between ∼12000 and 40000 cm^{-1} is presented in Figure 9. Two broad bands are observed, which can be immediately assigned as the $^3T_{1g}(F) \rightarrow {}^3T_{2g}$ and $^3T_{1g}(F) \rightarrow {}^3T_{1g}(P)$ (O_h) transitions, commonly observed in hexacoordinate vanadium(III) complexes. The spectrum may be satisfactorily reproduced as a superposition of four Gaussian functions, centered at energies given in Table 2. The 80 K reflectance spectrum of a powdered sample of CsVSH has been recently presented and discussed.[28] Bands at ∼9850, ∼12200 and ∼37600 were reported and assigned as d−d transitions. However, as these observations were not reproduced in our single-crystal study, we suggest that these bands have another origin. For example, a small amount of oxidation on the surface of the powder can distort the spectrum greatly, as the vanadyl ion gives rise to intense absorption bands in the near-infrared. In an earlier work, we reported the electronic spectrum of RbVSH.[8] Weak, narrow bands were observed in the near-infrared (NIR), which were assigned as a component of the $^3T_{1g} \rightarrow {}^1T_{2g}$ (O_h) transition. Analogous bands are observed in the spectra of CsVSH and CsVSD, presented in Figure 10. Assignments of the vibronic band follow by comparison with the emission spectrum

Table 3. Energies (cm^{-1}) and Assignments of Vibronic Bands Relative to the Electronic Origin of the $^3A_g \rightarrow {}^1E_g$ (S_6) Absorption Spectrum of RbVSH, CsVSH, and CsVSD

	RbVSH	CsVSH	CsVSD
lat(VO_6)	146, 176	104, 125, 143, 170, 180	103, 122, 142, 169, 180
ν_6(VO_6)	221, 252	219, 250	215, 244
ν_4(VO_6)	322	320, 333	304, 317
ν_3(VO_6)	546	546, 577	500, 523

CsCrSH[8] and are given in Table 3. The ligand-field analysis suggests that the vibronic structure is built on the $^3A_g \rightarrow {}^1E_g$ (S_6) electronic origin. The observation of this transition in the β-alums is of great consequence, as its energy can be precisely determined and is strongly dependent on the interelectronic-repulsion parameters, which provide a measure of the degree of delocalization of the valence electrons. The electronic origin is observed to shift to higher energy upon deuteriation, in agreement with luminescence measurements recently reported for the vanadium alums.[7] Transitions to other singlet states, expected in this region, were not observed.

The 15 K single-crystal electronic spectrum of GuVSH is presented in Figure 11 and is broadly in accordance with that reported previously.[29] The trigonal symmetry of the space group affords a rigorous definition of the electronic excited states, through measurements using polarized radiation. The bands corresponding to the $^3T_{1g}(F) \rightarrow {}^3T_{2g}$ and $^3T_{1g}(F) \rightarrow {}^3T_{1g}(P)$ (O_h) electronic transitions occur at higher energy compared to the cubic alums and exhibit extensive structure. Transition energies are listed in Table 2. No bands that could be assigned to transitions from triplet to singlet states were observed. However, a broad, weak band has been observed in luminescence at 10199(15) cm^{-1}, attributed to the $^3A_g \rightarrow {}^1E_g$ (S_6) electronic origin.[7]

3.3. Crystallographic Data. 3.3.1. Structural Data of CsVSH and RbVSH. Structure refinements were made using programs based on the Cambridge Crystallographic Subroutine Library.[30] It was evident in the first refinements that the observed intensities of the strongest reflections were reduced by extinction. The final refinement was therefore made against the unmerged normalized data with the wavelength of the individual observations included in the Becker and Coppens type-I model for secondary extinction.[31] Due to the regular forms of the crystals, the attenuation due to absorption is approximately equal for all reflections observed at the same wavelength, and the wavelength dependence of the absorption is then corrected in the empirical normalization to the same incident wavelength. Therefore, despite the considerably larger attenuation of the neutron beam due to the large proportion of hydrogen in the two samples, no explicit correction for absorption was required.

Owing to the small neutron scattering length of V, the thermal parameter for V was constrained to be the same as that for Cs. Since only relative cell dimensions can be extracted from LADI measurements, the bond lengths relating to the CsVSH structure were calculated using the cell parameter determined from SXD measurements (10 K) on CsVSD,[32] in conjunction with the fractional coordinates

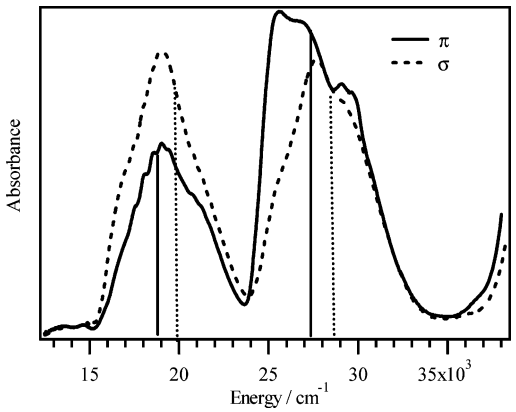

Figure 11. Single-crystal absorption spectrum of GuVSH, recorded at 15 K, in σ and π polarizations. The vertical lines correspond to the energies calculated for the C_3 site using the AOM.

obtained from LADI measurements at (15 K). For RbVSH, no low-temperature diffraction measurements, from which the unit cell parameter, *a*, can be estimated, are available. However, a fair estimate of the value of *a*, at 15 K, may be obtained by reducing the value, determined at 295 K,[14] by the same fraction as that found for CsVSH,[15,32] whence a value of 12.326 Å is obtained. Data collection and analysis parameters are given in Table 4, and selected interatomic distances and interbond angles are listed in Supporting Information, along with the final fractional coordinates and thermal parameters.

3.3.2. Structural Data of GuVSH. Guanidinium hexa-aqua vanadium(III) disulfate (GuVSH) crystallizes isotypically with guanidinium hexa-aqua aluminum disulfate[17] in a noncentrosymmetric space group, which implicates the calculation of the ratio of the symmetry-related domains. The refinement of this parameter (Flack x[33]) revealed that the crystals of GuVSH exist also as inversion twins (x = 0.52(2)). The X-ray diffraction structure of GuVSH is in close agreement with the previous structure determinations of GuAlSH and GuCrSH.[17] There are two crystallographically different $[V(H_2O)_6]^{3+}$ ions. The aqua ion on C_{3v} symmetry is located at the special position ([0, 0, 0]) while those of C_3 symmetry sit at the special position [$^1/_3$, $^2/_3$, z]. All hydrogen atoms could be located from Fourier difference synthesis maps and were refined under geometrical restraints. The bond distances and distances to the second next neighbors were included as parameters into the calculation, resulting in optimized geometry for guanidinium ions and aqua ligands, respectively. Data collection and analysis parameters are given in Table 4. Selected interatomic distances and interbond angles are listed in Supporting Information, along with the final fractional coordinates and thermal parameters.

3.3.3. The Structure of the $[V(OH_2)_6]^{3+}$ Cation in the Vanadium Alums and the Guanidinium Salt. In all the vanadium salts examined, the VO_6 framework is regular, with a small trigonal compression. There is little variation in the V−O bond lengths, listed in Table 5. This is important, since,

(33) Flack, H. D.; Bernardinelli, G. *Acta Crystallogr.* **1999**, A*55*, 908−915.

Table 4. Data Collection and Analysis Parameters for Measurements Performed on the Neutron and X-ray Diffractometers

	$CsV(SO_4)_2 \cdot 12H_2O$	$RbV(SO_4)_2 \cdot 12H_2O$	$[C(NH_2)_3][V(OH_2)_6](SO_4)_2$
diffractometer	LADI Laue diffractometer on a thermal-neutron beam		Rigaku AFC-7 three-circle diffractometer
detectors	cylindrical image plate detector 4000 × 2000 pixels, each 200 × 200 μm^2, cylinder sensitive area; 159 mm cylinder radius; ±144° in 2γ, ±52° in ν		Mercury70 CCD (2 × 2 bin mode, rectangular)
wavelength range	1.3−1.7 Å accepted	1.2−1.8 Å accepted	0.71073 Å
mol wt/g	592	544	411
cryst growth	aq solution	aq solution	aq solution
cryst form	near regular bipyramid	near regular bipyramid	near regular bipyramid
cryst size	2.7 × 2.3 × 1.8 mm^3	2.4 × 2.3 × 1.5 mm^3	0.42 × 0.40 × 0.28 mm^3
cryst syst	cubic	cubic	trigonal
space group	$Pa\bar{3}$ (No. 205)	$Pa\bar{3}$ (No. 205)	$P31m$ (No. 157)
Z	4	4	3
T (K)	15	15	292
a (Å)	12.411(3)[a]	12.326[a]	11.8116(4)
b (Å)			11.8116(4)
c (Å)			9.0311(3)
α (deg)	90	90	90
β (deg)	90	90	90
γ (deg)	90	90	120
V ($Å^3$)	1911.7	1872.7	1091.16(6)
ρ_{calc} ($g \cdot cm^{-3}$)	2.057	1.929	1.878
no. patterns	5	9	995
exposure time per pattern	45 min.	60 min	15 s/4 s
cryst rotation between exposures (deg)	25	15	0.6
obsd reflns	2690	7678	15473
unique reflns	684 ($I > 0$)	929 ($I > 0$)	2487 ($I > 0$); 2444 ($I > 2\sigma$)
abs coeff (cm^{-1})	n.a.	n.a.	1.045
refinement program	SFLSQ on F, $1/\sigma^2(F)$ weights		SHELXL-97 on F^2, $1/\sigma^2(F^2)$ weights
refined params	72	72	152
$R(F)$	0.118	0.142	0.0268
wR	0.056	0.065	0.0737
WR(F^2)	0.102	0.107	0.0744
S	2.40	2.93	1.114

[a] Unit cell parameters were determined indirectly, please see text for details.

Table 5. Transition Energies and Ground-State g Values of the $[V(OH_2)_6]^{3+}$ Cation, Calculated Using the Angular Overlap Model[a]

		CsVSH/ Cs[Ga:V]SH	GuVSH/ Gu[Ga:V]SH (C_{3v})	GuVSH/ Gu[Ga:V]SH (C_3)	RbVSH	CsVSD/ Cs[Ga:V]SD
AOM bonding		$e_\sigma = 6950$	$e_\sigma = 6950$	$e_\sigma = 6950$	$e_\sigma = 6950$	$e_\sigma = 6950$
params/cm^{-1}		$e_{\pi\perp} = 920$	$e_{\pi\perp} = 832, 920$	$e_{\pi\perp} = 915, 869$	$e_{\pi\perp} = 920$	$e_{\pi\perp} = 920$
		$e_{\pi\parallel} = 0$	$e_{\pi\parallel} = 0$	$e_{\pi\parallel} = 0$	$e_{\pi\parallel} = 0$	$e_{\pi\parallel} = 0$
V−O bond length/Å		2.003(2)	1.987(2)	1.993(2)	2.004(2)	1.996(2)
angles defining coordination geometry of water molecules/deg[b]	θ_1, θ_2	55.37(4) [124.63]	56.4(1), 124.6(1)	56.1(1), 124.5(1)	55.28(3) [124.71]	55.41(3) [124.59]
	ϕ_1, ϕ_2	0 [60]	0 [60]	0, 59.8(1)	0 [60]	0 [60]
	ψ_1, ψ_2	66.68(13) [−66.68]	[90], [−90]	86.2, −86.7	66.45(10) [−66.45]	66.82(6) [−66.82]
	α_1, α_2	0.4(2) [0.40]	18, 1	4, 14	1.4(2) [1.4]	0.6(1) [0.6]
spin-Hamiltonian		$D = 4.8580\ cm^{-1}$	$D = 3.5823\ cm^{-1}$	$D = 3.5768\ cm^{-1}$	$D = 4.9122\ cm^{-1}$	$D = 4.8277\ cm^{-1}$
params of ^3A (C_3) ground term		$g_\parallel = 1.9501$	$g_\parallel = 1.9558$	$g_\parallel = 1.9558$	$g_\parallel = 1.9498$	$g_\parallel = 1.9502$
		$g_\perp = 1.8655$	$g_\perp = 1.8992$	$g_\perp = 1.8996$	$g_\perp = 1.8642$	$g_\perp = 1.8663$
$k_\parallel = 1.00$, $k_\perp = 0.885$						
spinor levels and degeneracies of $^3E(C_3)$ {$^3T_{1g}(F)$, O_h} term		1845 e	2613 e	2618 e	1820 e	1860 e
		1954 e	2719 e	2724 e	1930 e	1969 e
		2052 a	2816 a	2822 a	2028 a	2066 a
		2062 a	2823 a	2829 a	2038 a	2076 a
energies and degeneracies of spinor levels arising from $^1T_{1g}$ and ^1E (O_h) terms		10214 e	10246 e	10239 e	10208 e	10216 e
		12133 e	12881 e	12891 e	12111 e	12145 e
		12404 a	13171 a	13173 a	12378 a	12419 a
energies and degeneracies of terms arising from higher lying $^3T_{2g}$ (O_h) term		18300	18700	18700	18300	18300
		19200	19800	19800	19200	19200
energies and degeneracies of terms arising from higher lying $^3T_{1g}$ (O_h) term		26700	27000	27000	26700	26700
		27600	28400	28400	27600	27600

[a] The angles θ, ϕ, and ψ are those used by Schäffer to define the angular geometry of the complex, with the quantization axis coincident with the 3-fold axis.[38,46] The angle α defines the angle between the V−O bond vector and the plane of the water molecule. The estimated errors in the angle ψ, which largely dictates the magnitude of the trigonal field, are shown in round brackets; the quantities in square brackets are generated by symmetry requirements. For all calculations, $B = 644$, $C = 2963$, $\zeta = 166.52\ cm^{-1}$. [b] The geometric parameters for the alkali-metal alums were calculated from neutron diffraction data. The geometric parameters for the guanidinium alum were calculated from X-ray diffraction data, as described in the text.

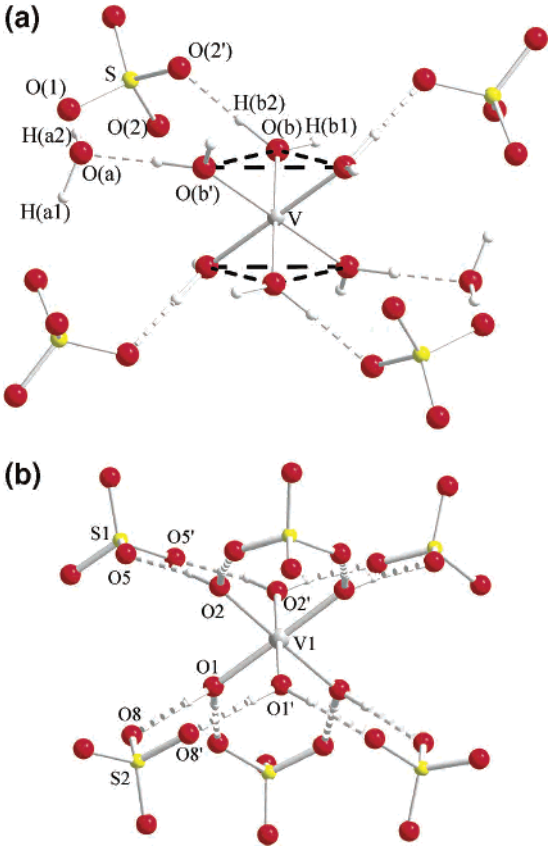

Figure 12. (a) Coordination geometry about the vanadium(III) cation in the β-alums, constructed from the 15 K neutron-diffraction data of CsVSD. (b) Coordination geometry about the vanadium(III) cation on the C_{3v} site, in GuVSH, constructed from the 292 K X-ray-diffraction data.

in deriving a set of AOM parameters for the $[V(OH_2)_6]^{3+}$ cation in one configuration, and then applying them to another, a minimal change in the 3d radial distribution function can be assumed. Further discussion of the structure of the VO_6 framework in salts containing the $[V(OH_2)_6]^{3+}$ cation is given in Supporting Information. The most pronounced difference in the stereochemistry of the $[V(OH_2)_6]^{3+}$ cation, between salts formed with guanidinium and those formed with an alkali metal as a counterion, lies in the disposition of the hydrogen atoms. The structures of the vanadium alums are in accordance with those previously determined for the cesium sulfate alums of Fe,[34] Ru,[35,36] Cr,[37] Mo,[36] and Ga.[32] The molecular geometry of the $[V(OH_2)_6]^{3+}$ cation in the β-alums is dictated largely by strong, linear hydrogen bonds formed with surrounding sulfate and water groups, and is shown in Figure 12a. The mode of water coordination is trigonal planar, with the water molecules rotated about the V−O bond vectors, to give overall S_6 symmetry. The stereochemistry may be defined in terms of the AOM angles, θ, ϕ, and ψ, relative to the unique 3-fold axis.[38] The angles θ and ϕ define the geometry of the VO_6 framework, and ψ defines the twist of the water molecules about the metal−oxygen bond vector. When the VO_6 framework is octahedral, a value of $\psi = 45°$ gives T_h symmetry, and $\psi = 90°$ all-horizontal D_{3d} symmetry. In the β-alums $\psi \sim 66°$, from neutron-scattering measurements. A similar value was inferred from an earlier X-ray study of the vanadium alums, by assuming, correctly, that the hydrogen bonds emanating from the tervalent cation are essentially linear.[14] The same procedure may be applied to the GuVSH salt, where only X-ray diffraction data are available and, hence, the positions of the hydrogen atoms are poorly defined. The disposition of the water molecules and sulfate anions about the vanadium(III) center on the C_{3v} site is shown in Figure 12b. In this instance, the C_{3v} site symmetry dictates that $\psi = 90°$, $-90°$ for the two unique water molecules. Analysis of the V−O···H···O−S hydrogen bond vectors for the cation on the C_3 site suggests similar values for ψ. The molecular geometries of the two crystallographically distinct $[V(OH_2)_6]^{3+}$ cations in GuVSH are thus both close to all-horizontal D_{3d} and are akin to that found for the $[V(OH_2)_6]^{3+}$ cation in the triflate salt,[39] the structure of which has been discussed extensively.[1,32,37] The AOM angles for the $[V(OH_2)_6]^{3+}$ cation in the β-alums, and on both sites in the GuVSH alum, are collected in Table 5. The table includes values for the tilt angle, α, defined as the angle between the V−O bond vector and the water plane. The neutron diffraction data of the β-alums are of very high-quality allowing the AOM angles to be defined very precisely; small differences are identified in the value of ψ, which are on the limit of significance. Further projections of the structures of CsVSH and GuVSH, displaying thermal ellipsoids, are given in Supporting Information.

4. Ligand-Field Analysis

The AOM is a semiempirical model that boasts an ability to inter-relate the electronic and molecular structure of transition-metal complexes, when the AOM bonding parameters for the metal−ligand interaction are known.[40] To put the model to the test, we first establish a set of parameters to describe the electronic structure of the $[V(OH_2)_6]^{3+}$ cation in CsVSH, and then examine whether these parameters account for the data obtained for other complexes. Calculations were undertaken using the program LIGFIELD, by Jesper Bendix.[41]

The energies of the excited-state ligand-field terms, along with the energies of the ligand-field components of the $^3T_{1g}$ ground term, determine the Racah and bonding parameters, and these are given in the caption of Table 5, along with ζ, which is set to a value so as to reproduce the zero-field-splitting parameter, D, of the $[V(OH_2)_6]^{3+}$ cation in CsVSH. The g-values can then be reproduced, but only by employing anisotropic orbital reduction factors: $k_{||} = 1.00$ and $k_{\perp} =$

(34) Best S. P.; Forsyth, J. B. *J. Chem. Soc., Dalton Trans.* **1990**, 395.
(35) Best S. P.; Forsyth, J. B. *J. Chem. Soc., Dalton Trans.* **1990**, 3507.
(36) Best S. P.; Forsyth, J. B.; Tregenna-Piggott, P. L. W. *J. Chem. Soc., Dalton Trans.* **1993**, 2711.
(37) Best S. P.; Forsyth, J. B. *J. Chem. Soc., Dalton Trans.* **1991**, 1721.
(38) Schäffer, C. E. *Struct. Bonding* **1968**, 5, 68−95.
(39) Cotton, F. A.; Fair, C. K.; Lewis, G. E.; Mott, G.; Moss, F. K.; Schultz, A. J.; Williams, M. J. *J. Am. Chem. Soc.* **1984**, *106*, 5319.
(40) Larsen, E.; La Mar, G. N. *J. Chem. Educ.* **1974**, *51*, 633−640. Figgis, B. N.; Hitchman, M. A. *Ligand Field Theory and its Applications*; Wiley-VCH: New York, 2000. Schoenherr, T.; Atanasov, M.; Adamsky, H. *Compr. Coord. Chem. II* **2004**, *2*, 443−455.
(41) Bendix, J. *Compr. Coord. Chem. II* **2004**, *2*, 673−676.

0.885. These parameters are now used as input for the calculation of the electronic structure of the two crystallographically distinct $[V(OH_2)_6]^{3+}$ cations of the GuVSH salt. The only modification made is to reduce the value of $e_{\pi\perp}$ according to the recommendation of Dubicki, that is $e_{\pi\perp}(\alpha) = e_{\pi\perp}(\alpha = 0)\cos^2(\alpha)$,[42] where α is the tilt angle, see Table 5. From comparison between the experimental and calculated energies given in Tables 2 and 5, the computed trigonal-field splitting of the $^3T_{1g}$ ground term, Δ, is seen to be in extremely good agreement with the electronic Raman data. The parameter Δ is dictated largely by the value of ψ, and the quantity $(e_{\pi\perp} - e_{\pi\parallel}) = 920(10)$ cm^{-1}. These results show that the AOM bonding parameters have genuine chemical significance, the metal−water π-bonding being dominated by the interaction normal to the plane of the water molecule for trigonal planar coordination. This inference is in accordance with an earlier polarized-neutron-diffraction study of the isostructural CsMoSD, which afforded the determination of the spin density throughout the $[Mo(OD_2)_6]^{3+}$ cation.[43]

When $\Delta \gg \zeta$, as is the case here, D is inversely proportional to Δ. The zero-field-splitting is calculated to be much lower in GuVSH compared to CsVSH, in accordance with the EPR measurements. The numerical values of D, given in Table 5, closely follow those calculated using the analytical expression below, formulated using standard methods of perturbation theory, utilizing an analytical expression for Δ,[37] and setting $e_{\pi\parallel}$ to zero

$$D \sim -\frac{[\delta(^3E_g)]^2}{12e_{\pi\perp}\{\cos(2\psi)\}} \qquad (10)$$

where $\delta(^3E_g)$ is the energy range spanned by the spinor levels of the ^3E_g(F) term. For GuVSH, where Raman transitions to the spinor levels of the ^3E_g(F) term are clearly resolved,[5] $\delta(^3E_g)$ is much smaller than the calculated value. It is curious that the widths of the electronic Raman bands observed for RbVSD and RbVSH are, respectively, too small and too large, with respect to expectations based on ligand-field theory.[4]

Another consequence of the increase in Δ is that the transitions to the higher-lying triplet states occur at higher energy. In Figure 11, the calculated energies of the components of the $^3T_{2g}$ and $^3T_{2g}$(F) terms of GuVSH are overlaid as vertical lines on top of the electronic absorption spectrum. While the AOM gives a good prediction of the barycenter of the $^3T_{2g}$ and $^3T_{2g}$(F) terms, the asymmetric band profiles are clearly not in accordance with the calculated trigonal field splittings of the excited triplet terms. Inspection of Tables 2 and 5 shows that this is also true for CsVSH, a discrepancy previously noted for the ammonium vanadium alum, and imputed to excited-state Jahn−Teller effects.[44] The same conclusion has been drawn from analysis of the $^3T_{1g} \rightarrow {}^3T_{2g}$ (O_h) electronic absorption band profile of $[V(OH_2)_4Cl_2]^+$.[45]

The calculated shifts in the parameters D and Δ, and in the energy of the lower-lying ^1E state, on replacing Cs with Rb are in impressive agreement with the experimental data. This may be fortuitous, as differences between the AOM angles, the all-important angle ψ in particular, are at the limit of being statistically significant.

In all the cesium alums, the parameter, D, is reduced upon deuteriation. The energy of the lower-lying ^1E state is also significantly different, being found at higher energy in CsVSD. The differences, though small, are not borne out of the AOM calculations. To reproduce the change in the energy of the lower lying ^1E state upon deuteriation requires a slightly different choice of Racah parameters, suggesting that deuteriation has a small impact upon the metal−water bonding interaction. By altering ζ or $(e_{\pi\perp} - e_{\pi\parallel})$, D can be reproduced, with a marginal change in the g values. The marked increase in the value of $g_\parallel$ for Cs[Ga:V]SH upon deuteriation then necessitates that a different value of $k_\parallel$ be employed.[24] However, the change in g values for the Cs[Al:V]SH and Cs[In:V]SH alums upon deuteriation is more modest, and the spin-Hamiltonian parameters for these systems can be interpreted with orbital reduction factors consistent with those given in Table 5. Though contrary to a hand-waving rationale of chemical bonding, the inequality $k_\parallel > k_\perp$ is in accordance with the polarized-neutron-diffraction study of CsMoSD,[43] from which it was established that spin transfer from the metal to the ligand occurred primarily through depletion of spin density in the components of the π-bonding orbitals with densities perpendicular to the plane of the water molecules. Nevertheless, we stress that the orbital reduction factors should not be overinterpreted. As the last parameters which we vary, they simply absorb the drastic assumptions of the model, such as isotropic spin−orbit coupling and Racah parameters, and the approximations used in the formulation of the AOM.

5. Summary and Conclusion

Spectroscopic and crystallographic studies of salts containing the $[V(OH_2)_6]^{3+}$ cation have enabled the elucidation of the ground- and excited-state electronic structure, to unprecedented precision, in well-defined molecular geometries, providing a rigorous test of the ability of the AOM to interrelate the electronic and molecular structure of transition-metal complexes.

It is found that the AOM provides a remarkably good account of the inter-relation between the disposition of the water molecules about the vanadium(III) cation and the

(42) Riesen H.; Dubicki, L. *Inorg. Chem.* **2000**, *39*, 2206.
(43) Best, S. P.; Figgis, B. N.; Forsyth, J. B.; Reynolds, P. A.; Tregenna-Piggott, P. L. W. *Inorg. Chem.* **1995**, *34*, 4605−4610.
(44) Hitchman, M. A.; McDonald, R. G.; Smith, P. W.; Stranger, R. *J. Chem. Soc., Dalton Trans.* **1988**, 1393.
(45) Bussière, G.; Beaulac, R.; Cardinal-David, B.; Reber, C. *Coord. Chem. Rev.* **2001**, *219−221*, 509−543.
(46) The AOM rotation operator, $R(\psi, \theta, \phi)$, defined in ref 38, is as follows: With reference to a space-fixed Cartesian coordinate system *XYZ*, with the metal−water bond vector directed along the *Z*-axis, we first rotate around *Z* by the angle, ψ, then around *Y* by the angle, θ, and finally around *Z* by the angle ϕ. In previous publications,[8,24,37] the rotation of the water molecules about the M−O vector has been defined in terms of the angle φ that the plane of the water molecule makes relative to the MO_6 framework. φ is fomally defined in ref 8. When the MO_6 framework is perfectly octahedral, $\psi° = 45° - \varphi°$.

trigonal field splitting of the $^3T_{1g}$ ground term, which impacts on all the spectroscopic quantities. This provides the chemist with confidence that the AOM bonding parameters do indeed have a genuine chemical significance and may be applied to give a reasonable prediction of the electronic structure for a complex of known geometry. Nevertheless, while the AOM gives an accurate prediction of the barycentered-energies of the ligand-field terms, the calculated energies of the components do not render an adequate account of the positions of the band maxima. The discrepancy between experiment and ligand field theory is most acute in the absorption spectrum of GuVSH. Excited-state Jahn−Teller effects are known to have a profound effect on the band-shapes and polarization characteristics of the electronic spectra of transition metal ions,[47] and we shall consider the manifestation of the phenomena on the electronic absorption spectra of vanadium(III) complexes in a future publication. The influence of dynamic Jahn−Teller coupling on the electronic Raman profiles and ground-state spin-Hamiltonian parameters are considered in the next paper.

Acknowledgment. This work was funded by the Swiss National Science Foundation. The corresponding author is particularly grateful for the award of an exchange fellowship that facilitated a visit to the Department of Chemistry, at the University of Copenhagen. We thank Dr. H. Borrmann, MPI CPFS Dresden, for the X-ray data collection.

Supporting Information Available: Tables of fractional co-ordinates, thermal parameters, selected interatomic bond lengths, as well as further information on the stereochemistry of the $[V(OH_2)_6]^{3+}$ cation, additional EPR spectra, and further theoretical work relating to the derivation of eqs 6−9. Crystallographic data in CIF format. This material is available free of charge via the Internet at http://pubs.acs.org.

IC049292L

(47) Al Haroun, A.; Culiuc, L. L.; Mirovitskii, V. Y.; Nateprov, A. N.; Palii, A. V.; Tezlevan, V. E.; Tsukerblat, B. S. *Proc. SPIE Int. Soc. Opt. Eng.* **2002**, *4766* (Spectroscopy of Crystals Activated by Rare-Earth and Transition-Metal Ions), 248−260.